Feynman diagrams and Fano interference in light scattering from doped semiconductors

1997 J. Phys.: Condens. Matter 9 5965

(http://iopscience.iop.org/0953-8984/9/27/022)

J. Phys.: Condens. Matter **9** (1997) 5965–5976. Printed in the UK PII: S0953-8984(97)82515-5

Feynman diagrams and Fano interference in light scattering from doped semiconductors

V I Belitsky†, A Cantarero†‖, M Cardona†, C Trallero-Giner‡ and S T Pavlov§

† Max-Planck-Institut für Festkörperforschung, Heisenbergstrasse 1, D-70569 Stuttgart, Germany
‡ Department of Theoretical Physics, Havana University, Havana, Cuba
§ P N Lebedev Physical Institute, Russian Academy of Sciences, 117924 Moscow, Russia

Received 10 March 1997

Abstract. We present a diagrammatic approach to the calculation of quantum interference contributions to the Raman light scattering efficiency of doped semiconductors. A three-band model within a parabolic approximation is used to account for the electronic and optical phonon Raman scatterings under the condition of resonance coupling of an optical phonon with an inter-valence-band electronic continuum. Diagram techniques allow us to compare the roles of various processes contributing to an asymmetrical scattering profile.

1. Introduction

An interesting phenomenon of quantum interference between discrete and continuum types of material excitations has attracted the attention of many research groups. Fano-type asymmetric profiles were observed in Raman scattering from doped semiconductors by Cerdeira *et al* [1] after its theoretical description by Fano [2]. During the last few years renewed interest in the problem was stimulated by observations of Fano profiles in the magneto-absorption spectra of GaAs [3, 4]. The basic physics of the effect has been well understood in terms of interference between elementary amplitudes when more than one different but energetically overlapping final states in a spectroscopic process couple to each other via some residual interaction.

Theoretical models [5–9] of different complexity have been applied to calculate the Fano profiles for various types of excitation process, with optical techniques playing a special role. Both simplified phenomenological approaches [5] and full-scale microscopic calculations [6, 7] have been used to attack the problem. The well known two-parameter phenomenological analytic expression for Fano profiles usually gives a good fit to the data. However, the details of the interference effects, which depend strongly on the types of process involved, are hidden behind such a fitting procedure, that applies equally to different but formally similar situations. On the other hand, the full microscopic analysis, which for solids includes the details of the band structure and interaction parameters, requires considerable effort, and can usually be carried out only through advanced numerical calculations. Therefore, giving full credit to both approaches, we give here an example of an 'intermediate' method, which is rather far from a full microscopic treatment, but takes into account the most important dependences of all of the parameters on the relevant

‖ Permanent address: University of Valencia, 46100 Burjasot (Valencia), Spain.

0953-8984/97/275965+12$19.50

quantum numbers and frequencies, and thus preserves the individuality of the process under consideration. We see the advantage of our approach in the fact that all of the equations are integrated analytically, allowing us to compare easily the different contributions to the scattering efficiency. Moreover, the diagrammatic approach gives a very clear physical picture of the quantum interference effects which lead to the Fano profiles. Preliminary aspects of this work were reported in reference [10].

The paper is organized as follows. A brief description of the diagram techniques is given in section 2. In section 3 we derive the equations for one-optical-phonon and electronic Raman scattering efficiencies, taking into account final-state interactions and quantum interference effects, leading to the Fano profiles. A discussion and conclusions are presented in section 4, while the appendix includes some bulky algebraic expressions used to calculate the scattering efficiencies.

2. Diagram techniques

The light scattering efficiency can be written in terms of the fourth-rank light scattering tensor $S_{\alpha\gamma\beta\lambda}(\omega_l, \omega_s, \kappa_l, \kappa_s)$ as [11]

$$\frac{\mathrm{d}^2 S}{\mathrm{d}\Omega\ \mathrm{d}\omega_s} = \frac{\omega_s^3 \omega_l}{c^4} \frac{n_s}{n_l} e^*_{s\alpha} e_{s\beta} e_{l\gamma} e^*_{l\lambda} S_{\alpha\gamma\beta\lambda}(\omega_l, \omega_s, \kappa_l, \kappa_s) \tag{1}$$

where ω_l (ω_s), n_l (n_s), and $\boldsymbol{e}_l$ ($\boldsymbol{e}_s$) are the frequency, the refractive index, and the polarization vector of the incident (scattered) light, respectively. The tensor $S_{\alpha\gamma\beta\lambda}(\omega_l, \omega_s, \kappa_l, \kappa_s)$ can be evaluated with the help of diagram techniques similar to those developed for calculating the scattering efficiency of a multi-phonon Raman process [11]. This technique is directly related to Fermi's Golden Rule and, as a result, gives a very clear and intuitive picture of the quantum interference between various possible contributions to the scattering amplitude. The diagrams to be evaluated in the next section are shown in figures 1 and 2.

The definition of the final state in the scattering process plays a principal role in our approach. It is labelled as the vertical section F in all of the diagrams for scattering efficiency (not scattering amplitude!) in figures 1 and 2. Any line on the left of the final state F must be substituted for with the corresponding retarded Green's function for electronic $\mathrm{i}G(\omega, \boldsymbol{k})$ and vibrational $\mathrm{i}D(\omega, \boldsymbol{q})$ excitations, whereas the lines on the right-hand side of the final state correspond to the advanced propagators $(-\mathrm{i})G^*(\omega, \boldsymbol{k})$ and $(-\mathrm{i})D^*(\omega, \boldsymbol{q})$, respectively. The vertices of electron–phonon interaction on the left-hand side are $(-\mathrm{i}/\hbar)M(\boldsymbol{q})$ and $(-\mathrm{i}/\hbar)M^*(\boldsymbol{q})$ for emission and absorption of a phonon $\boldsymbol{q}$, respectively, where $M(\boldsymbol{q})$ is a corresponding matrix element. On the right-hand side of the final-state section one has to change the factor $(-\mathrm{i}/\hbar)$ to $(\mathrm{i}/\hbar)$. The difference $\mathrm{i}[G(\omega, \boldsymbol{k}) - G^*(\omega, \boldsymbol{k})]$ must substitute for each possible electronic final state, whereas $\mathrm{i}[D(\omega, \boldsymbol{q}) - D^*(\omega, \boldsymbol{q})]$ corresponds to the phonon final state. Note that for *bare propagators* these differences lead to the δ-functions determining the energy conservation. The interested reader will find more details on the diagram technique rules in references [11, 12].

3. Scattering efficiency

We employ these diagram techniques to calculate the light scattering efficiency of a p-doped zinc-blende-like semiconductor whose band structure is modelled by one conduction and two valence parabolic bands as shown in the lower panel of figure 3. The level of doping is such that resonant coupling between an optical (O) phonon and direct inter-valence-band

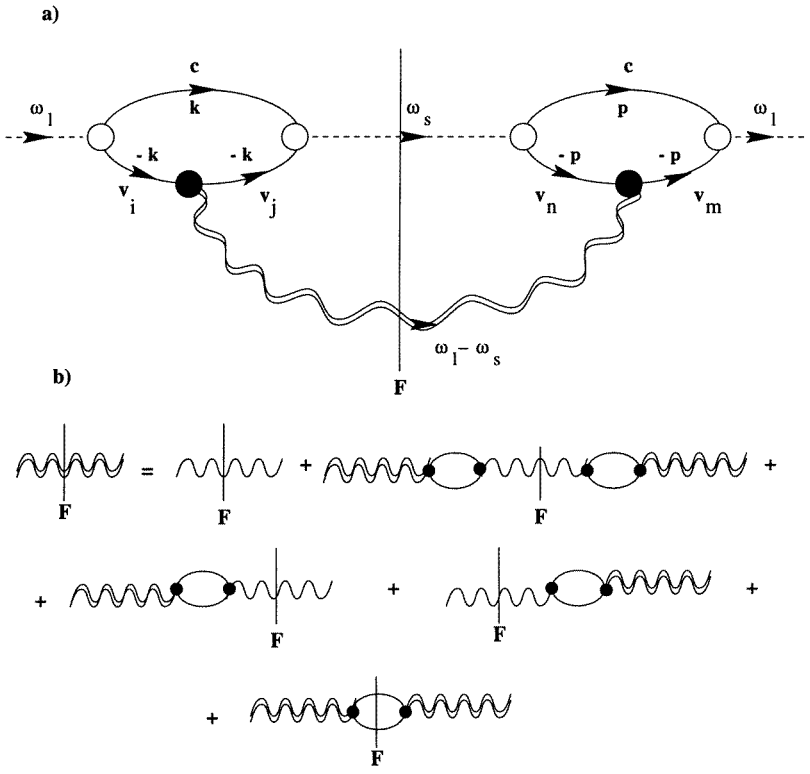

Figure 1. (a) The diagram for the scattering efficiency of a one-phonon Raman process. The final state is indicated by the vertical section F which crosses the line of the renormalized phonon and that of the scattered photon. (b) The diagram representation of the renormalized final-state propagator expressed through the bare propagators of the electronic and phonon excitations.

(IVB) electronic excitations leads to a strong mixing of both states in the range where they are degenerate in energy. Obviously, the conventional perturbation theory fails to describe the process adequately in this case, and one has to solve the Dyson equation for renormalized propagators.

First, we calculate one-O-phonon Raman scattering, assuming electron–phonon interaction of the deformation potential type. After that, pure electronic contributions to the scattering efficiency, producing the necessary continuum, are taken into account. The quantum interference of amplitudes for pure electronic and one-phonon processes occurs via the electron–phonon coupling, and it leads to spectra with Fano line-shapes. For the profile evaluations below, we use $m_c = 0.5m_0$, $m_1 = 0.5m_0$, $m_2 = 0.15m_0$ for the effective masses of the conduction and higher and lower valence bands, respectively, $n_p \sim 10^{20}$ cm^{-3} for the hole concentration, and $E_g = 3.4$ eV for the fundamental gap ($\Gamma_{25'} \rightarrow \Gamma_{15}$). This corresponds approximately to the experimental data of reference [1] for Si.

3.1. One-phonon Raman scattering

A one-O-phonon process is possible only through the $\boldsymbol{A} \cdot \boldsymbol{p}$ term in the electron–photon Hamiltonian which has to be evaluated to second order in perturbation theory. The Feynman diagram for the scattering efficiency is shown as figure 1(a), where the double wavy line

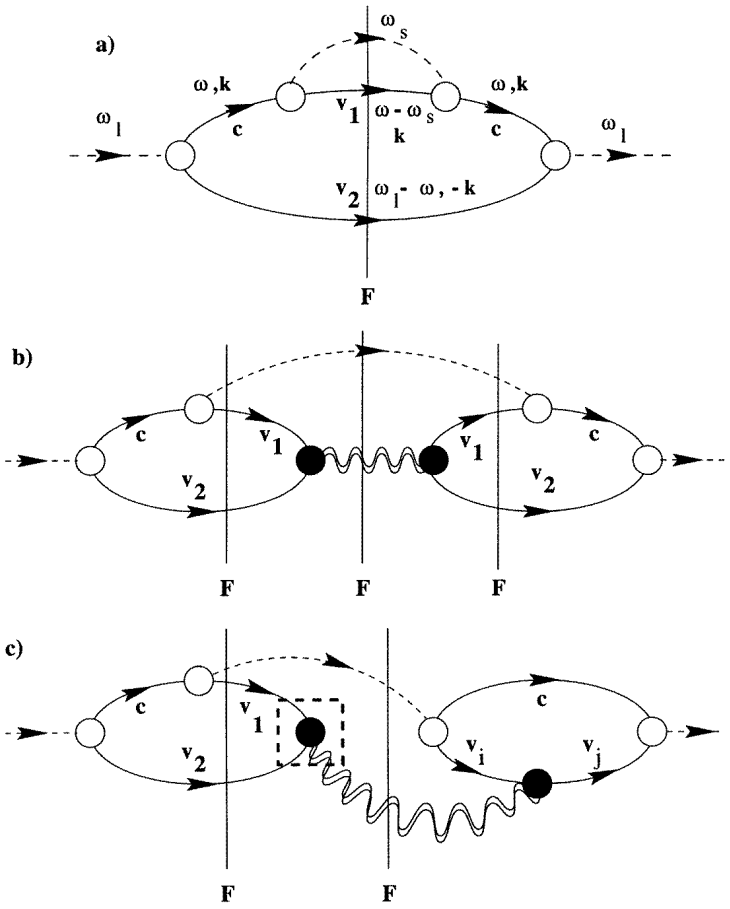

Figure 2. (a) The lowest-order contribution to the electronic scattering efficiency following from the $\boldsymbol{A} \cdot \boldsymbol{p}$ term in the light–matter interaction Hamiltonian. (b) The RPA diagram corresponding to the final-state-interaction contribution to the efficiency of the electronic Raman scattering. (c) The diagram responsible for the quantum interference of the one-phonon and electronic Raman processes. The vertices of electron–phonon interaction coupling the two processes to each other are shown in the dashed box. Two final states in the diagram have to be taken into account while evaluating the scattering efficiency.

represents the renormalized propagator of the O phonon, which includes an infinite sequence of transitions between the bare O phonon and the polarization loop of IVB excitations in the RPA approximation. The use of the renormalized O-phonon propagator implicitly assumes that not only bare phonons but also bare IVB electronic excitations participate to form the final states in the scattering process. This point is illustrated by the identity for the renormalized final-state propagator $\mathrm{i}[D(\omega) - D^*(\omega)]$ represented by the diagrams given as figure 1(b). This identity shows how the difference $\mathrm{i}[D(\omega) - D^*(\omega)]$ is composed of the contributions from bare electronic and phonon final states, including all terms to infinite order in the RPA approximation. Note that the last term in this series corresponds to a pure electronic final state. The proof of this identity is rather straightforward when all renormalized phonon propagators in figure 1(b) are expanded in the RPA series.

With the help of the diagram techniques described above, the scattering efficiency of a

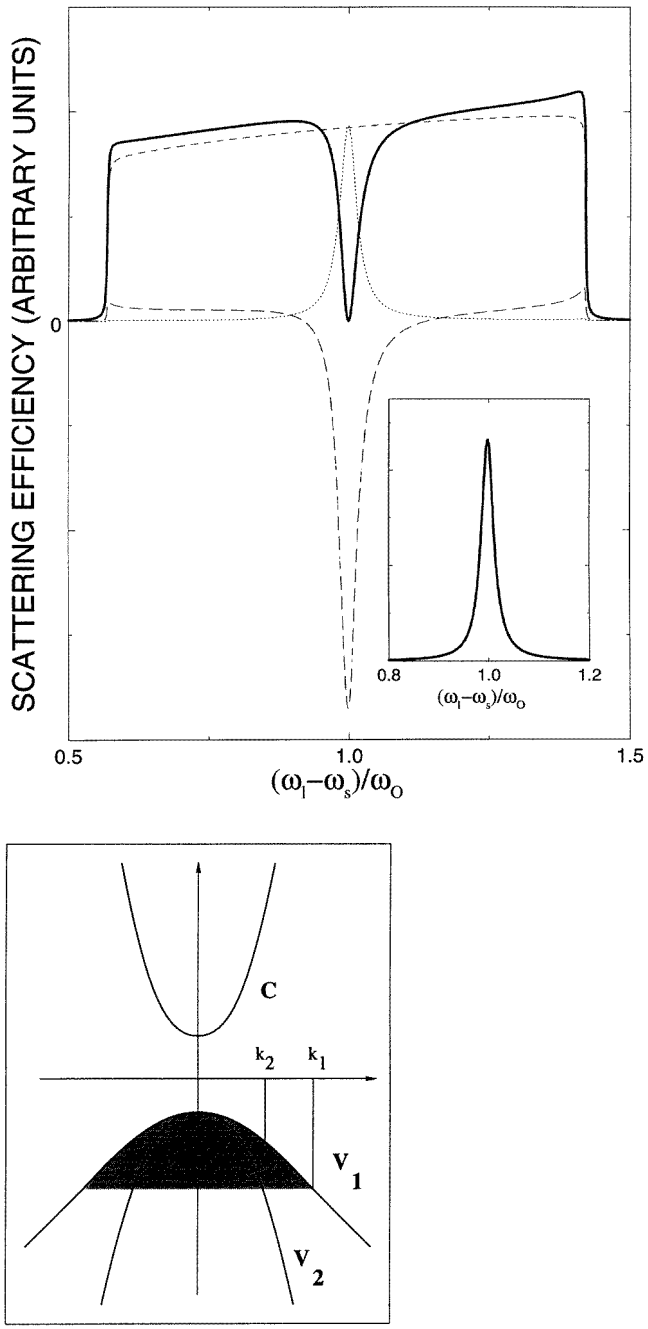

Figure 3. The scattering profiles corresponding to the phonon (dotted line) and electronic (long-dashed line) final states of the diagrams in figure 2(b) which account for final-state interactions in the electronic Raman process. The bare electronic scattering intensity and the sum of all of the contributions from figures 2(a) and 2(b) are shown as the dashed and solid curves, respectively. The schematic band structure and the one-phonon scattering efficiency according to the diagram given as figure 1(a) are represented in the lower panel and right-hand-side inset, respectively.

one-O-phonon process is found to be

$$\frac{\mathrm{d}^2 S_R}{\mathrm{d}\Omega\ \mathrm{d}\omega_s} = \mathcal{R}\sigma_0 \left[\mathrm{i}(D(\varrho) - D^*(\varrho))\right] |P(\omega_l, \omega_s)|^2 \tag{2}$$

where $\varrho = \omega_l - \omega_s$, and the scattering amplitude consists of four terms:

$$\begin{aligned} P(\omega_l, \omega_s) = {} & \Psi^{21}_{k_1}(Z^l_2(\gamma_c, \gamma_2), Z^s_1(\gamma_c, \gamma_1)) + \Psi^{12}_{k_1}(Z^l_1(\gamma_c, \gamma_1), Z^s_2(\gamma_c, \gamma_2)) \\ & + \Psi^{11}_{k_1}(Z^l_1(\gamma_c, \gamma_1), Z^s_1(\gamma_c, \gamma_1)) + \Psi^{22}_{k_2}(Z^l_2(\gamma_c, \gamma_2), Z^s_2(\gamma_c, \gamma_2)) \end{aligned} \tag{3}$$

which take account of the deformation-potential-induced intra-valence-band transitions (Ψ^{11} and Ψ^{22}) and transitions between upper and lower valence bands (Ψ^{12} and Ψ^{21}) with the emission of an O phonon (see the lower panel of figure 3). The function $\Psi^{ij}_{k_l}$ is defined in equation (A4). We have also used the following definitions:

$$\sigma_0 = \frac{\omega_s}{\omega_l}\frac{n_s}{n_l} \left|\boldsymbol{p}^*_{cv} \cdot \boldsymbol{e}_l\right|^2 \left|\boldsymbol{p}_{cv} \cdot \boldsymbol{e}^*_s\right|^2 \left(\frac{e}{m_0}\right)^4 \frac{1}{(2\pi)^3 c^4 \hbar^2 \omega_O^3 l_{ph}^3} \tag{4}$$

and

$$\mathcal{R} = \frac{1}{(2\pi)^2}\left(\frac{|V|}{\hbar\omega_O}\right)^2 \frac{V_0}{l_{ph}^3} \qquad l_{ph} = \sqrt{\frac{\hbar}{2m_0\omega_O}} \tag{5}$$

where V and V_0 are the deformation potential constant and the normalization volume, respectively. The renormalized phonon propagator at zero wave vector is

$$\begin{aligned} \mathrm{i}D(\varrho) &= \frac{1}{\left[\mathrm{i}D_0(\varrho)\right]^{-1} - \mathrm{i}\Pi(\varrho)} \\ \mathrm{i}D_0(\varrho) &= \frac{\mathrm{i}\omega_O}{\varrho - \omega_O + \mathrm{i}0^+} \end{aligned} \tag{6}$$

where $D_0(\varrho)$ is dimensionless bare phonon propagator, the polarization loop is given by

$$\mathrm{i}\Pi(\varrho) = \mathrm{i}\mathcal{R}\beta\left[2(k_1 - k_2) + Z_3(\gamma_1, \gamma_2)\ln\frac{(Z_3(\gamma_1, \gamma_2) - k_1)}{(Z_3(\gamma_1, \gamma_2) + k_1)}\frac{(Z_3(\gamma_1, \gamma_2) + k_2)}{(Z_3(\gamma_1, \gamma_2) - k_2)}\right] \tag{7}$$

and the Fermi wave vectors in the two valence bands are

$$k_1 = l_{ph}(3\pi^2 n_1)^{1/3} \qquad k_2 = \sqrt{\frac{m_2}{m_1}}k_1 \tag{8}$$

where n_1 is the hole concentration in the upper valence band. We need to define three types of dimensionless wave vector which are used to express the scattering efficiencies:

$$\begin{aligned} Z^t_i(\Gamma_1, \Gamma_2) &= \sqrt{\mu_i\left(\frac{\omega_t - \omega_g}{\omega_O} + \mathrm{i}\frac{\Gamma_1 + \Gamma_2}{2\omega_O}\right)} \\ Z_3(\Gamma_1, \Gamma_2) &= \sqrt{\beta\left(\frac{\omega_l - \omega_s}{\omega_O} + \mathrm{i}\frac{\Gamma_1 + \Gamma_2}{2\omega_O}\right)} \end{aligned} \tag{9}$$

$$\mu_i = \frac{1}{m_0}\frac{m_c m_i}{m_c + m_i} \qquad \beta = \frac{1}{m_0}\left(\frac{1}{m_2} - \frac{1}{m_1}\right)^{-1} \tag{10}$$

where $i = 1$ or 2, and t has to be substituted for with l and s for incident and scattered light, respectively. The phenomenological broadenings Γ_1, Γ_2 stand for the broadenings γ_1, γ_2, and γ_c of the states in the two valence bands and in the conduction band, respectively. The broadening γ_c should only be important when the frequency of the incident light allows for real excitation across the fundamental gap.

The result from the calculations using equation (2) for $\hbar\omega_l = 2$ eV is shown in the right-hand-side inset of figure 3 where the one-phonon line is broadened by interaction with IVB excitations. The broadening has been taken into account self-consistently through the imaginary part of the polarization operator in equations (6) and (7).

3.2. Electronic Raman scattering

Below the resonance with the fundamental gap, the scattering profile of a pure electronic contribution must follow the density of states of IVB electronic excitations. The diagram for the lowest-order electronic contribution to the scattering efficiency is shown as figure 2(a); it corresponds to the $\boldsymbol{A}\cdot\boldsymbol{p}$ term in the light–material interaction Hamiltonian, while the $\boldsymbol{A}^2$ term gives a negligible contribution to the Raman scattering by IVB excitations. The corresponding scattering efficiency is

$$\frac{\mathrm{d}^2 S_{el}}{\mathrm{d}\Omega\ \mathrm{d}\omega_s} = \sigma_0 F(\omega_l, \omega_s) \tag{11}$$

where the function $F(\omega_l, \omega_s)$ results from the bulky but straightforward integration over the $\boldsymbol{k}$-vector, and is defined in equation (A1). An example of the scattering profile for the pure electronic contribution calculated according to equation (11) is represented by the flat dashed curve in figure 3 for $\hbar\omega_l = 2$ eV. As expected, it follows the density of the IVB electronic excitations which produce the continuous background needed for Fano interference.

3.3. Final-state interaction

The so-called final-state interaction (FSI) takes into account a possible coupling of the final state to other material excitations. It expresses the fact that the basis of states chosen to calculate the scattering efficiency does not diagonalize the complete material Hamiltonian. In our case, the basis of free electron–hole pairs (EHPs) gives a good choice in the range of energies far from the energy of the O phonon. The FSI with optical phonons leads then to the broadening of electronic states. However, in the range where the EHP energy overlaps the energy of the O phonon, the effect of the FSI goes far beyond the simple broadening, and the Dyson equation for the renormalized propagator has to be solved for a certain class of diagrams.

The FSI contribution to the electronic Raman scattering is shown as figure 2(b). It is important to distinguish between the phonon and EHP final states which give the additive contributions to the spectrum. Therefore, the diagram given as figure 2(b) gives three contributions. Two of them describe the interference terms with the bare EHP in the final state, and the third one corresponds to the excitation of the renormalized phonon. The corresponding equations were integrated analytically, yielding

$$\frac{\mathrm{d}^2 S_{ph}}{\mathrm{d}\Omega\ \mathrm{d}\omega_s} = \mathcal{R}\sigma_0 \left[\mathrm{i}(D(\varrho) - D^*(\varrho))\right] |\Sigma(\omega_l, \omega_s)|^2 \tag{12}$$

$$\Sigma(\omega_l, \omega_s) = \mu_2 \beta \Phi(Z_2^l(\gamma_c, \gamma_2), Z_3(\gamma_1, \gamma_2)) \tag{13}$$

$$\frac{\mathrm{d}^2 S_{el}}{\mathrm{d}\Omega\ \mathrm{d}\omega_s} = -\mathcal{R}\sigma_0 \left[\mathrm{i}D(\varrho)\right]^* \Sigma(\omega_l, \omega_s)\Theta(\omega_l, \omega_s) + \mathrm{CC} \tag{14}$$

where Θ and Φ are defined in equations (A2) and (A3), respectively.

The contributions to the scattering profile from the processes of figure 2(b) which end in either electronic or O-phonon excitations are shown in figure 3 by the long-dashed and dotted lines, respectively. The peak of the contribution from the O-phonon final state

is always positive, and can be seen as indirect one-phonon Raman scattering. However, it can be taken into account only together with two interference contributions from the electronic final state which are negative. One can see from figure 3 that the sum of all three contributions from figure 2(b) actually gives a negative anti-resonance. The total profile for electronic scattering taking into account both bare final states (figure 2(a)) and final states renormalized by the FSI (figure 2(b)) is shown by the solid line in figure 3. The scattering efficiency is positive for all frequencies, as it should be. In the range far from the frequency of the O phonon it follows approximately the density of the IVB excitations. However, at $\varrho \sim \omega_O$, the profile deviates from the electronic density of states, and the scattering intensity vanishes following strong renormalization of the continuum. A zero value of the scattered intensity means that the electronic component of the renormalized final state is negligible when $\varrho \simeq \omega_O$. The sum of the contributions in figures 2(a) and 2(b) corresponds to the case of $T_p = 0$ in standard notation [5], where the Fano parameter q would be equal to zero if the real part of the polarization operator were negligible. This however is not the case, and the real part of the self-energy is responsible for an asymmetry of the scattering profile which depends on the energy position of the O phonon within the electronic continuum. Note that the FSI results in the vanishing of the scattering efficiency at $\varrho = \omega_O$, as it should for $T_p = 0$.

3.4. Interference contributions

So far we have not considered quantum interference between the processes of one-O-phonon and electronic Raman scattering. Obviously, one cannot speak of direct interference of two amplitudes which lead to different final states, since that contradicts the principles of quantum mechanics. Therefore, in such a scenario, it is implicitly assumed that some interaction couples the two processes to each other. In our consideration, it is the electron–phonon interaction which joins the two amplitudes in figure 2(c) into one diagram for the scattering efficiency. The corresponding vertex is indicated by the dashed box. Thus, the two contributions for two possible final states must be taken into account for the interference diagram given as figure 2(c).

For obtaining the correct position of the minimum in a scattering profile, it is very important to take into account the sign of the two vertices of interaction with an O phonon. The first one (in a dashed box) corresponds to the phonon-assisted inter-valence-band *electron–hole* recombination, whereas the second indicates the scattering of a *hole* by an O phonon either within the same valence band or in the inter-valence-band transition. The opposite sign of the two vertices does not play any role in the contributions of the diagrams given as figures 1, 2(a), and 2(b), where the vertices of each type only occur as pair products. However, for the interference contribution given as figure 2(c), the relative sign is very important as regards determining the sign of the Fano parameter q.

All interference contributions can be separated into two parts, corresponding to the EHP and phonon final states according to the diagram given as figure 2(c). They can be written as

$$\frac{\mathrm{d}^2 S_{el}}{\mathrm{d}\Omega\ \mathrm{d}\omega_s} = -\mathcal{R}\sigma_0 \left[\mathrm{i}D(\varrho)\right] P(\omega_l, \omega_s)\Theta^*(\omega_l, \omega_s) + \mathrm{CC} \tag{15}$$

and

$$\frac{\mathrm{d}^2 S_{ph}}{\mathrm{d}\Omega\ \mathrm{d}\omega_s} = \mathcal{R}\sigma_0 \left[\mathrm{i}(D(\varrho) - D^*(\varrho))\right] \Sigma^*(\omega_l, \omega_s) P(\omega_l, \omega_s) + \mathrm{CC}. \tag{16}$$

An example of calculations for the contributions of figure 2(c) is shown in figure 4(a) for the phonon (dotted line) and EHP (dashed line) final states. The total sum of all of the

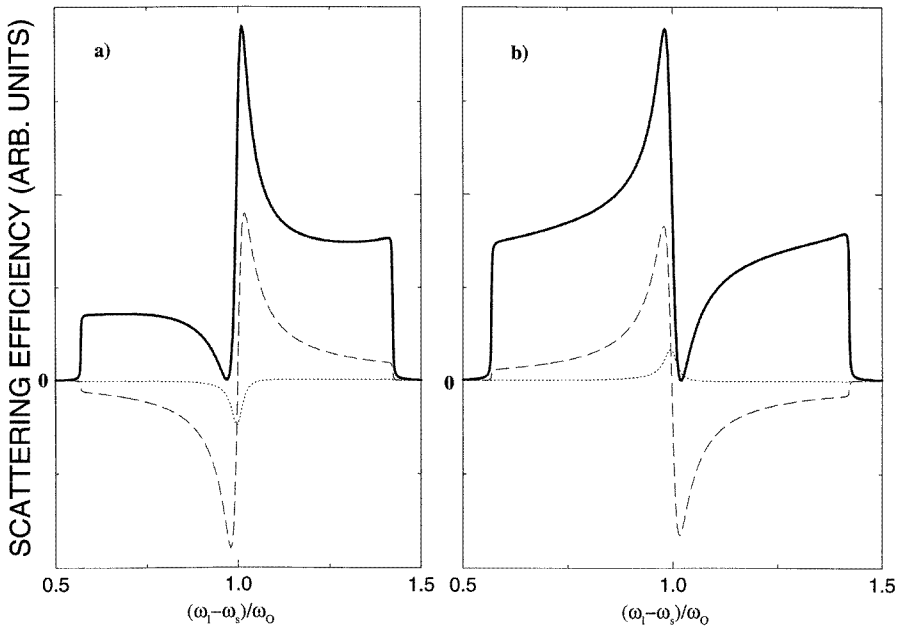

Figure 4. The contributions of the diagram given as figure 2(c) for (a) positive and (b) negative relative signs of the one-phonon and electronic Raman amplitudes. The contributions for phonon (dotted line) and electronic (dashed line) final states are shown separately. Solid lines represent the sum of all of the contributions from figures 1 and 2. The signs of the Fano parameters are opposite for the two cases.

contributions calculated in this section is shown as a solid line in figure 4(a), to demonstrate that the scattering efficiency vanishes on the lower-frequency side of the phonon peak, which corresponds to the positive sign of the effective Fano parameter q, in agreement with the experimental situation in p-Si [1].

4. Discussion and conclusions

Although the electronic contributions to the scattering amplitude result from a well defined region of the Brillouin zone where the doping level allows for vertical transitions between the two valence bands (see the lower panel of figure 3), the one-phonon amplitude can gain contributions from different areas of $\boldsymbol{k}$-space. Therefore, the relative phase of the two interfering amplitudes may depend on the full details of the band structure. For illustration, we show in figure 4(b) the result of calculations for the case where the relative sign of the two vertices of interaction with the O phonon in figure 2(c) is opposite to that for the p-doped Si used for the calculations of figure 4(a). The minimum occurs on the higher-frequency side of the one-phonon peak that corresponds to a negative q. Note that this is the situation found for n-type Si [13].

In order to compare our results with the data of reference [1] we have to incorporate in our model the fact that the resonance behaviour of a one-O-phonon Raman amplitude is mainly determined by the high density of EHP excitations along the [111] direction—the so-called E_1-gaps. A rough accounting for that fact can be achieved by scaling the one-O-phonon amplitude for different laser frequencies, so as to achieve a correspondence

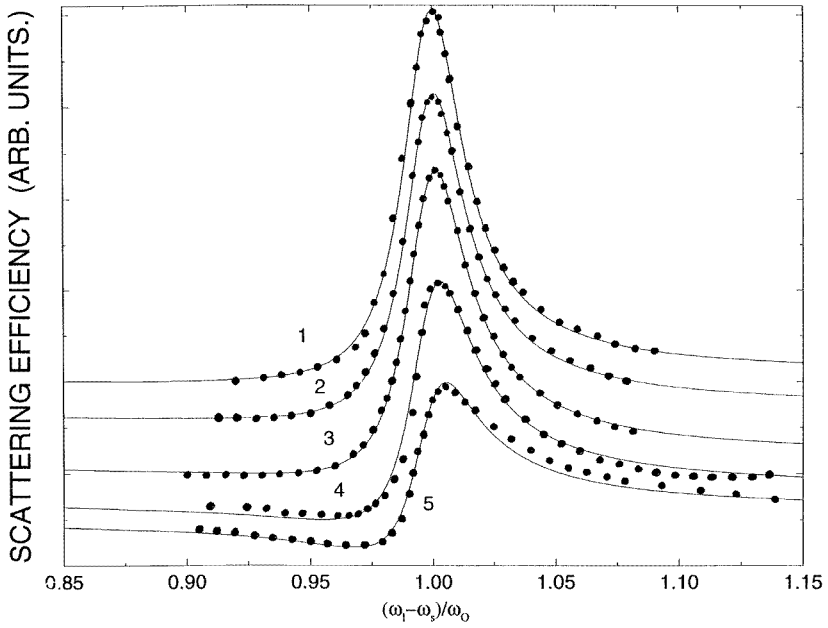

Figure 5. The results of calculations for a number of laser frequencies, together with the data of reference [1] (see the text for details).

with the experimental results for pure Si [14]. In figure 5 we show the theoretical set of curves together with experimental data of reference [1] for different incident frequencies: 1: 2.75 eV; 2: 2.55 eV; 3: 2.4 eV; 4: 2.2 eV; and 5: 1.9 eV. To fit the data, we had to increase the one-O-phonon amplitude by a factor of 5 going from lower to higher laser frequency. The fit of the experimental data with the well known Fano expression corresponds, however, to a factor-of-3.5 increase in the Fano parameter q. This means that the direct application of our model, which neglects the specific band structure along the [111] direction (i.e. the two-dimensional E_1-gaps), would give a small decrease of the effective Fano parameter instead of the increase observed in reference [1]. This is because the excitation across the $\Gamma_{25'} \rightarrow \Gamma_{15}$ fundamental gap in a parabolic model results in a rather weak dependence of both electronic and one-O-phonon Raman amplitudes when the frequency is within the interval 1.9–2.75 eV. A small decrease of q means that the electronic amplitude grows even faster than that of the one-O-phonon process that follows from the integration over $\boldsymbol{k}$-vectors.

Finally, there can be a situation where a Raman phonon is emitted through intra-band Fröhlich interaction, while the resonant FSI can only occur via deformation-potential-induced IVB transitions. In such a case, the two contributions from figure 2(c) exactly compensate each other. This compensation emphasizes the general rule which does not allow interference between the real and imaginary interactions. The total profile is then the sum of the two positive terms: the electronic contributions (including the FSI) and the one-phonon Raman intensity. The scattering efficiency does not vanish at the minimum, and the position of the minimum with respect to the phonon peak depends on the behaviour of the real part of the polarization operator.

To summarize, the analytical equations for the light scattering efficiencies of a p-doped semiconductor have been derived within the parabolic approximation for one

conduction and two valence bands. The roles of the final-state interaction and the quantum interference between one-phonon and electronic Raman processes have been analysed through application of diagram techniques which take into account self-consistently the renormalization of electronic and vibrational excitations in the final state of a scattering process. Typical examples of the corresponding scattering profiles have been calculated.

Acknowledgments

VIB thanks the European Union and the Max Planck Gesellschaft for financial support, and the University of Valencia and the Max Planck Institute for their hospitality. Thanks are also due to P Santos for a critical reading of the manuscript. This work was partially supported by Russian Fundamental Investigation Fund (96-02-17115-a, 95-02-04184-a) and by the 'Physics of semiconductor nanostructures' Programme (1-009).

Appendix A. Definition of $F(\omega_l, \omega_s)$ and $\Theta(\omega_l, \omega_s)$

The scattering efficiency of the pure electronic process given as figure 2(a) is essentially determined by the function

$$\begin{aligned} F(\omega_l, \omega_s) = -\frac{\omega_O}{\gamma_c}\{&\mu_1\mu_2[\Phi(Z_1^s(-\gamma_c, \gamma_1), Z_2^l(-\gamma_c, -\gamma_2)) \\ &+ \Phi(Z_1^s(-\gamma_c, -\gamma_1), Z_2^l(-\gamma_c, \gamma_2)) \\ &- \Phi(Z_1^s(-\gamma_c, \gamma_1), Z_2^l(-\gamma_c, \gamma_2)) - \Phi(Z_1^s(-\gamma_c, -\gamma_1), Z_2^l(-\gamma_c, -\gamma_2))] \\ &+ \mu_1\beta[\Phi(Z_1^s(\gamma_1, -\gamma_c), Z_3(-\gamma_1, \gamma_2)) + \Phi(Z_1^s(\gamma_1, \gamma_c), Z_3(-\gamma_1, -\gamma_2)) \\ &- \Phi(Z_1^s(\gamma_1, \gamma_c), Z_3(-\gamma_1, \gamma_2)) - \Phi(Z_1^s(\gamma_1, -\gamma_c), Z_3(-\gamma_1, -\gamma_2))] \\ &+ \mu_2\beta[\Phi(Z_2^l(\gamma_2, -\gamma_c), Z_3(\gamma_2, \gamma_1)) + \Phi(Z_2^l(\gamma_2, \gamma_c), Z_3(\gamma_2, -\gamma_1)) \\ &- \Phi(Z_2^l(\gamma_2, \gamma_c), Z_3(\gamma_2, \gamma_1)) - \Phi(Z_2^l(\gamma_2, -\gamma_c), Z_3(\gamma_2, -\gamma_1))]\} \end{aligned} \tag{A1}$$

whereas

$$\begin{aligned} \Theta(\omega_l, \omega_s) = &-\mu_1\beta\Phi(Z_1^s(\gamma_1, \gamma_c), Z_3(-\gamma_1, \gamma_2)) + \mu_1\beta\Phi(Z_1^s(\gamma_1, \gamma_c), Z_3(-\gamma_1, -\gamma_2)) \\ &- \mu_2\beta\Phi(Z_2^l(\gamma_2, \gamma_c), Z_3(\gamma_1, \gamma_2)) + \mu_2\beta\Phi(Z_2^l(\gamma_2, \gamma_c), Z_3(-\gamma_1, \gamma_2)) \end{aligned} \tag{A2}$$

is used to express all contributions via the $\boldsymbol{A}\cdot\boldsymbol{p}$ term with the electronic final state.

The functions

$$\begin{aligned} \Phi(Z(\Gamma_1, \Gamma_2), \tilde{Z}(\tilde{\Gamma}_1, \tilde{\Gamma}_2)) = &\frac{1}{\tilde{Z}^2(\tilde{\Gamma}_1, \tilde{\Gamma}_2) - Z^2(\Gamma_1, \Gamma_2)} \\ &\times \left[Z(\Gamma_1, \Gamma_2)\ln\frac{k_1 - Z(\Gamma_1, \Gamma_2)}{k_2 - Z(\Gamma_1, \Gamma_2)}\frac{k_2 + Z(\Gamma_1, \Gamma_2)}{k_1 + Z(\Gamma_1, \Gamma_2)}\right. \\ &\left. - \tilde{Z}(\tilde{\Gamma}_1, \tilde{\Gamma}_2)\ln\frac{k_1 - \tilde{Z}(\tilde{\Gamma}_1, \tilde{\Gamma}_2)}{k_2 - \tilde{Z}(\tilde{\Gamma}_1, \tilde{\Gamma}_2)}\frac{k_2 + \tilde{Z}(\tilde{\Gamma}_1, \tilde{\Gamma}_2)}{k_1 + \tilde{Z}(\tilde{\Gamma}_1, \tilde{\Gamma}_2)}\right] \end{aligned} \tag{A3}$$

and

$$\begin{aligned} \Psi_w^{ij}(Z(\Gamma_1, \Gamma_2), \tilde{Z}(\tilde{\Gamma}_1, \tilde{\Gamma}_2)) = &\frac{\mu_i\mu_j}{\tilde{Z}^2(\tilde{\Gamma}_1, \tilde{\Gamma}_2) - Z^2(\Gamma_1, \Gamma_2)} \\ &\times \left[Z(\Gamma_1, \Gamma_2)\ln\frac{w + Z(\Gamma_1, \Gamma_2)}{w - Z(\Gamma_1, \Gamma_2)} - \tilde{Z}(\tilde{\Gamma}_1, \tilde{\Gamma}_2)\ln\frac{w + \tilde{Z}(\tilde{\Gamma}_1, \tilde{\Gamma}_2)}{w - \tilde{Z}(\tilde{\Gamma}_1, \tilde{\Gamma}_2)}\right] \end{aligned} \tag{A4}$$

have been introduced to simplify the equations for the scattering efficiencies.

References

[1] Cerdeira F, Fjeldly T A and Cardona M 1973 *Phys. Rev.* B **8** 4734
[2] Fano U 1961 *Phys. Rev.* **124** 1866
[3] Glutsch S, Siegner U and Chemla D S 1994 *Phys. Rev.* B **50** 17 009
[4] Bellani V, Pérez E, Zimmermann S, Viña L, Hey R and Ploog K 1996 *Solid State Commun.* **97** 459
[5] Klein M V 1983 *Light Scattering in Solids, I* ed M Cardona (Heidelberg: Springer) p 147
[6] Arya K, Kanehisa M A, Jouanne M, Jain K P and Balkanski M 1979 *J. Phys. C: Solid State Phys.* **12** 3843
[7] Wallis R F and Balkanski M 1986 *Many-Body Aspects of Solid State Spectroscopy* (Amsterdam: North-Holland)
[8] Bechstedt F and Peuker K 1975 *Phys. Status Solidi* b **72** 743
[9] Ipatova I P and Subashiev A V 1976 *Fiz. Tverd. Tela* **18** 2145 (Engl. Transl. 1976 *Sov. Phys.–Solid State* **18** 1251)
[10] Belitsky V I, Trallero-Giner C, Cantarero A, Pavlov S T and Cardona M 1996 *Proc. 23rd Int. Conf. on the Physics of Semiconductors (Berlin)* vol 1, ed M Scheffler and R Zimmerman (Singapore: World Scientific) p 309
[11] Ivchenko E L, Lang I G and Pavlov S T 1977 *Fiz. Tverd. Tela* **22** 1751 (Engl. Transl. 1977 *Sov. Phys.–Solid State* **19** 718)
[12] Belitsky V I, Cardona M, Lang I G and Pavlov S T 1992 *Phys. Rev.* B **46** 15 767
[13] Chandrasekhar M, Renucci J B and Cardona M 1978 *Phys. Rev.* B **17** 1623
[14] Compaan A and Trodahl H J 1984 *Phys. Rev.* B **29** 793